PROCEEDINGS A

royalsocietypublishing.org/journal/rspa

Research

Cite this article: Vona M, Lauga E. 2025 Rotational mobility in spherical membranes: the interplay between Saffman–Delbrück length and inclusion size. *Proc. R. Soc. A* **481**: 20240473.
https://doi.org/10.1098/rspa.2024.0473

Received: 24 June 2024
Accepted: 7 January 2025

Subject Category:
Physics

Subject Areas:
fluid mechanics, mathematical physics

Keywords:
membrane, mobility, inclusion, Saffman–Delbrück

Author for correspondence:
Eric Lauga
e-mail: e.lauga@damtp.cam.ac.uk

Rotational mobility in spherical membranes: the interplay between Saffman–Delbrück length and inclusion size

Marco Vona and Eric Lauga

Department of Applied Mathematics and Theoretical Physics, University of Cambridge, Cambridge, UK

MV, 0000-0001-6497-5868; EL, 0000-0002-8916-2545

The mobility of particles in fluid membranes is a fundamental aspect of many biological and physical processes. In a 1975 paper (Saffman PG, Delbrück M. 1975 Brownian Motion in Biological Membranes. *Proc. Natl Acad. Sci. USA* **72**, 3111–3113. (doi:10.1073/pnas.72.8.3111)), Saffman and Delbrück demonstrated how the presence of external Stokesian solvents is crucial in regularizing the apparently singular flow within an infinite flat membrane. In the present paper, we extend this classical work and compute the rotational mobility of a rigid finite-sized particle located inside a spherical membrane embedded in Stokesian solvents. Treating the particle as a spherical cap, we solve for the flow semi-analytically as a function of the Saffman–Delbrück (SD) length (ratio of membrane to solvent viscosity) and the solid angle formed by the particle. We study the dependence of the mobility and flow on inclusion size and SD length, recovering the flat-space mobility as a special case. Our results will be applicable to a range of biological problems including rotational Brownian motion, the dynamics of lipid rafts, and the motion of aquaporin channels in response to water flow. Our method will provide a novel way of measuring a membrane's viscosity from the rotational diffusion of large inclusions, for which the commonly used planar Saffman–Delbrück theory does not apply.

THE ROYAL SOCIETY PUBLISHING

1. Introduction

The mobility of macroscopic inclusions located inside fluid membranes plays a role in many physical and biological processes, such as the kinetics of liquid domains in giant unilamellar vesicles [1,2] (figure 1A), the formation of finite-sized compartments in surface monolayers consisting of multiple chemical components [6,7], the kinetics of colloids adsorbed on liquid droplets [4] (figure 1B), the rotational diffusion of membrane-bound polymers [5] (figure 1C) and particles [8], and the postulated motion of aquaporin channels [9–11] in response to water flow [10] (figure 1D). Biological membranes often display curvature [12], which may be either intrinsic [13] or the result of stochastic fluctuations, as seen for example in the 'flicker phenomenon' of erythrocytes [14]. The prediction of particle mobility therefore requires formulating a hydrodynamic theory for flows inside curved membranes.

In the absence of shear orthogonal to the membrane [13,15], as in the case of lipid bilayers [16,17], it is appropriate to model membranes as two-dimensional fluids subject to internal viscous stresses and embedded within three-dimensional fluids referred to as solvents [15,18–23]. These solvents are coupled to the membrane by the no-slip and stress-balance boundary conditions [19,20] which, unlike for a simple fluid–fluid interface, must also account for the membrane viscous stresses [24–26]. As often done, we consider the case of membranes that are incompressible and impermeable to the solvents [21,27].

The presence of the solvents is not only biologically relevant, but also offers a resolution to the mathematical issues connected with translational mobility in an infinite membrane. Without solvents, a particle embedded in an infinite flat membrane would not have a well-defined translational mobility, due to the Stokes paradox [28]. Indeed, the two-dimensional Stokes flow around a body diverges logarithmically when the force on the body is nonzero, resulting in a theoretically infinite mobility. A resolution to the paradox was offered by Saffman and Delbrück in a classical paper [15]. They showed that the coupling to the viscous solvents below and above the membrane regularizes the problem by introducing a natural cut-off length scale for the logarithmic divergence, now known as the Saffman–Delbrück length and given by $\ell_{\mathrm{SD}} \equiv \eta/\mu$, where η is the two-dimensional membrane viscosity and μ is the solvent viscosity [29]. The features of the flow then strongly depend on the relative magnitude of the Saffman–Delbrück length and the other length scales in the problem (e.g. local radius of curvature, particle size) [27,30]. Note that membrane inertia, or the finite size of the membrane, may also be used to regularize the problem [15]. Saffman and Delbrück's discovery sparked a flurry of activity on particle mobility in different biological setups and geometries [19,31], including spherical [32,33] or tubular [34] membranes. Further studies considered slender [35,36] or active [37] inclusions, rigid boundaries inside the ambient fluids [6], the effect of membrane deformability [12,17] and elasticity [38]. Finally, some studies considered the possibility of partial embeddings, with membrane inclusions protruding into the solvents [39–41]. In all cases, solutions to the hydrodynamic problem must account for the extreme variability in inclusion size, which may range from that of a single peptide or lipid (about 10 nm in size) to larger bodies such as protein aggregates [36,42] and liquid domains (0.3–10 μm in radius) [2,3,43].

In this paper, we study the rotational mobility problem semi-analytically in the case of a finite-sized rigid particle within an incompressible spherical membrane. This is the situation illustrated schematically in figure 2A. Our primary motivation concerns the rotational motion of particles embedded in spherical vesicles [44], a situation relevant to the movement of ATP synthase [45], aquaporin channels [9–11], as well as the Brownian motion of membrane-embedded particles [46,47], and proteins of arbitrary size [36,42,48]. As we see below, the calculation carried out in the paper is valid more broadly in all cases where a rigid particle is made to rotate inside a spherical membrane (or 'vesicle'), itself embedded in a viscous solvent. Note that our work extends the work from [27] by allowing the particle to have a size comparable with the membrane.

The structure of the paper is as follows: in §2, we first outline a mathematical model for the particle-membrane-solvent system and summarize the methodology for solving the resulting equations. In §3, we focus on the results for the rotational mobility of the particle and the resulting

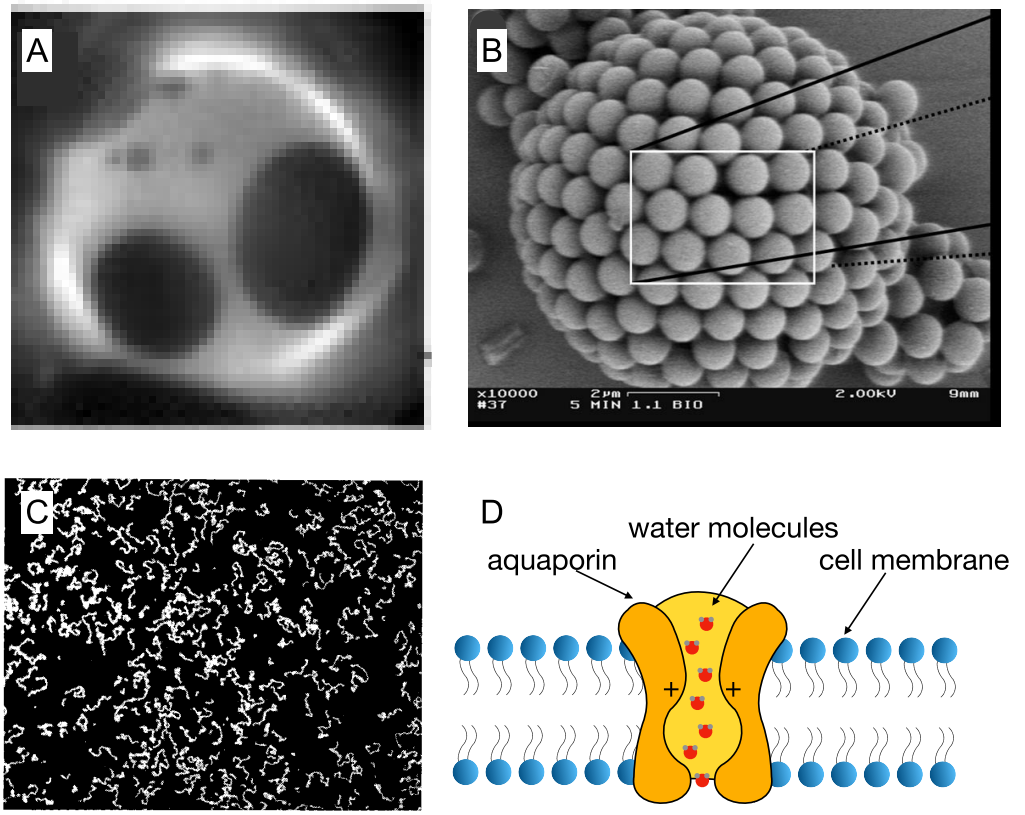

Figure 1. Diverse experimental examples of membrane inclusions: (A) Liquid domains (0.3–10 μm in radius) in giant unilamellar vesicles (15–50 μm in radius), with darker regions corresponding to higher viscosity [3]. (B) Colloids adsorbed on the fluid–fluid interfaces of emulsion droplets may be locked together to form a selectively permeable capsule [4]. (C) Semidilute solution of DNA electrostatically bound to a cationic lipid membrane and diffusing in-plane [5]. (D) Schematic representation of a human aquaporin, which facilitates efficient and specific passive permeation of water and other small uncharged solutes across the cell membrane. In this paper, we concern ourselves with rigid inclusions only.

membrane flow as a function of the dimensionless parameters governing the problem (§3a) and on the asymptotic values of the rotational mobility for scenarios involving a small or large particle, comparing our findings with the results obtained in previous studies (§3b). We finish with a summary of our findings and a discussion of potential extensions in §4.

2. Mathematical model

(a) Physical setup

The motivating examples listed in §1 concern the dynamics of a rigid particle inside a spherical membrane (vesicle). The mathematical setup for our calculation is illustrated in figure 2B. The membrane forms a sphere of radius R_m surrounded by Newtonian solvents (both inside and outside) of viscosity μ. The particle is modelled as a rigid spherical cap of curvilinear radius R_p and polar half-angle $\theta_p = R_p/R_m$, and its angular velocity is denoted by Ω. In the case of an incompressible, impermeable, Newtonian membrane [17,20] of viscosity η, our goal is to compute the total torque exerted on the particle.

In what follows, we describe the three-dimensional space with spherical coordinates $x^i = \{r, \theta, \phi\}$. We use the standard orthonormal vectors $\{\mathbf{e}_r, \mathbf{e}_\theta, \mathbf{e}_\phi\}$ as a local basis in the solvents, and

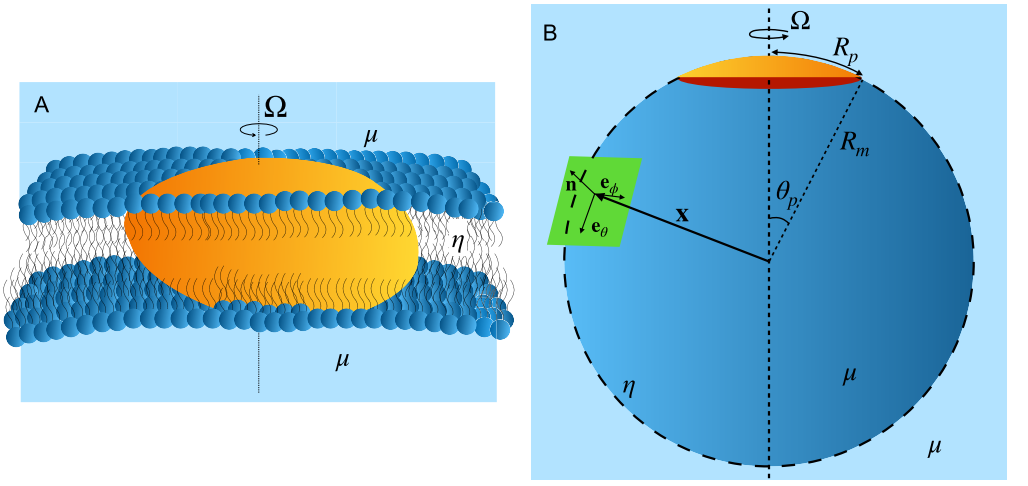

Figure 2. (A) Schematic of the experimental system under consideration, the rotation of a particle (orange structure) located inside a curved lipid bi-layer membrane (dark blue) that is embedded in a viscous solvent on both sides (light blue). (B) Schematic depiction of the mathematical problem. The rigid particle is modelled as a spherical cap of half-angle $\theta = \theta_p$ and curvilinear radius R_p inside a spherical membrane (vesicle) of radius R_m and rotating with angular velocity Ω. The membrane is endowed with spherical polar coordinates θ, ϕ with corresponding orthonormal basis vectors $\mathbf{e}_\theta, \mathbf{e}_\phi$, and local unit normal $\mathbf{n}$.

$\{\mathbf{e}_\theta, \mathbf{e}_\phi\}$ as a local orthonormal basis on the membrane. We assume that the membrane velocity is purely tangential, and denote the fluid velocities in the membrane and the solvents as $\mathbf{v}$, $\mathbf{V}^\pm$, respectively. From here onwards, a + superscript denotes the exterior of the membrane, and a − superscript denotes the interior.

(b) Mathematical model

(i) Field equations and matching conditions

For an incompressible membrane with a purely tangential velocity field, mass conservation in the membrane and the solvents takes the form [20,26]

$$\nabla \cdot \mathbf{v} = 0, \quad \overline{\nabla} \cdot \mathbf{V} = 0, \tag{2.1}$$

where ∇, $\overline{\nabla}$ are the gradient operators on the membrane and the solvents, respectively. In order to avoid infinite stresses, the inner and outer flows $\mathbf{V}^-$ and $\mathbf{V}^+$ must also satisfy the no-slip condition on the membrane

$$\mathbf{V}^\pm = \mathbf{v} \quad \text{(membrane)}. \tag{2.2}$$

Within the framework of continuum mechanics, forces in the membrane and the surrounding solvents (both assumed Newtonian [17,20]) are described by contravariant stress tensors $\boldsymbol{\sigma}$, $\boldsymbol{\sigma}^\pm$ given in an orthonormal vector basis by the constitutive relationships [17,20,27]

$$\boldsymbol{\sigma} = -p\mathbf{I}_2^\sharp + \eta\left[\nabla\mathbf{v} + (\nabla\mathbf{v})^{\mathrm{T}}\right]^\sharp \quad \text{(membrane)}, \tag{2.3}$$

$$\boldsymbol{\sigma}^\pm = -P^\pm\mathbf{I}_3^\sharp + \left[\overline{\nabla}\mathbf{V}^\pm + (\overline{\nabla}\mathbf{V}^\pm)^{\mathrm{T}}\right]^\sharp \quad \text{(solvents)}. \tag{2.4}$$

Here p, $P^\pm$ denote the membrane and ambient pressures, while η, μ are the membrane and ambient viscosities, respectively. A $\sharp$ denotes the index-raising sharp operator [17], and $\mathbf{I}_2$ and $\mathbf{I}_3$ are the (1, 1) identity tensors in the membrane and in the solvents.

Note that in a membrane, unlike in three-dimensional space, stresses correspond to forces per unit length, rather than per unit area. As a result, $[p] = \mathrm{Nm}^{-1}$ and $[\eta] = \mathrm{Nsm}^{-1}$, so that $\ell_{SD} = \eta/\mu$ has dimensions of length. The physical interpretation of ℓ_{SD} becomes apparent by considering an area patch of velocity U and size L, comparable with the typical length scale of the flow. The viscous force exerted by the solvents on the patch scales as $f_s \sim \mu UL$, while the force imparted by the membrane is of order $f_m \sim \eta U$. The drag from the solvents therefore dominates when $f_s \gg f_m \Leftrightarrow L \gg \ell_{SD}$ and the Saffman–Delbrück length may therefore be thought of, intuitively, as the cross-over size between two-dimensional membrane dynamics and three-dimensional bulk dynamics [3,49].

Force balance in the solvents is expressed by the standard Stokes equation $\nabla \cdot \boldsymbol{\sigma}^{\pm} = \mathbf{0}$, or

$$\mu \overline{\nabla}^2 \mathbf{V}^{\pm} = \overline{\nabla} P^{\pm}. \tag{2.5}$$

Similarly, we require force balance on every membrane area patch. These forces consist of membrane in-plane stresses and the traction forces $\mathbf{T} = (\boldsymbol{\sigma}^{+} - \boldsymbol{\sigma}^{-}) \cdot \mathbf{n}$ exerted by the solvents [17,42]. Force balance then takes the form

$$\mathrm{div}_s(\boldsymbol{\sigma}) + \mathbf{T} = \mathbf{0}, \tag{2.6}$$

where div_s denotes the surface divergence (see Appendix A). Further decomposing $\mathbf{T} = \boldsymbol{\tau} + T^n \mathbf{n}$, with $\boldsymbol{\tau}$ tangent to the membrane, the normal and tangent components of equation (2.6) may be recast into the following field equations [17,23,25]

$$\eta(\nabla^2 \mathbf{v} + G\mathbf{v}) - \nabla p^{\sharp} + \boldsymbol{\tau} = \mathbf{0}, \tag{2.7}$$

$$T^n + \boldsymbol{\sigma} : \mathbf{K} = 0. \tag{2.8}$$

Here, $\mathbf{K}$ is the (covariant) extrinsic curvature tensor, $G = \det(\mathbf{K})$ is the local Gaussian curvature and ∇^2 is the surface Laplacian. Physically, the $G\mathbf{v}$ term in the tangential force balance (2.7) reflects the fact that membrane shear may occur as a result of streamlines coming together due to curvature.

(ii) Axisymmetric solution

Because the setup is rotationally symmetric, the membrane flow $\mathbf{v}$ and the solvent flows $\mathbf{V}^{\pm}$ must be everywhere parallel to $\mathbf{e}_{\phi}$. Indeed, the flow in the solvents cannot have any r or θ component since they must change sign under reflections in a plane containing the z-axis (equivalent to reversing the sense of rotation of the particle). A similar symmetry argument shows that the tangential solvent stress $\boldsymbol{\tau}$ on the membrane must be purely in the ϕ direction, and that the normal component T^n coincides with the pressure jump across the membrane, i.e. $T^n = P^{-} - P^{+}$. Finally, because the only input in this problem is the angular velocity Ω, which is a pseudo-vector, by linearity of the Stokes equations there cannot be any pressure gradients in the membrane or the solvents. Therefore, the membrane and solvent pressures p and $P^{\pm}$ must be constants.

On account of these observations, only the azimuthal component of the membrane Stokes equation (2.7) is non-trivial. Given the identity $\mathbf{K} = -R_m^{-1}\mathbf{I}_2^{\flat}$ in a spherical membrane with a local orthonormal basis (with $\flat$ denoting the index-lowering flat operator [17]), the normal force balance in (2.8) simplifies to

$$\begin{aligned} 0 &= T^n + \boldsymbol{\sigma} : \mathbf{K} \\ &= P^{-} - P^{+} - R_m^{-1}\boldsymbol{\sigma} : \mathbf{I}_2^{\flat} \\ &= P^{-} - P^{+} + 2R_m^{-1}p. \end{aligned} \tag{2.9}$$

Notice that we used the incompressibility condition $\nabla\mathbf{v} : \mathbf{I}_2^{\flat} = 0$ (see equation (2.1)) in the last step. The constant membrane pressure therefore acts like a negative tension, imposing a capillary-like pressure jump.

For the purpose of solving the non-trivial ϕ component of equation (2.7), we choose to write the velocity field in a particular form, which simplifies later equations: we let $\mathbf{v} = R_m v(\theta)\sin(\theta)\mathbf{e}_\phi$, $\mathbf{V}^\pm = V^\pm(r,\theta) r\sin(\theta)\mathbf{e}_\phi$. In this formalism, the functions v and $V^\pm$ correspond to the fluid's local angular velocity about the z-axis, rather than the linear velocity. Substituting this axisymmetric ansatz into equation (2.7), we obtain the ordinary differential equation

$$\eta(v''\sin\theta + 3v'\cos\theta) + R_m\tau^\phi = 0 \quad \theta_p < \theta \le \pi \text{ (membrane)}, \tag{2.10}$$

$$v \equiv \Omega \quad 0 \le \theta \le \theta_p \text{ (particle)}. \tag{2.11}$$

Note that this equation may also be obtained by considering the standard Stokes equation in a thin spherical annulus, assuming that the thickness-integrated body force balances with external shear (see Appendix B).

(c) Legendre polynomial expansion

Following the classical squirmer solution [50], we decompose the three flows in a basis of Legendre polynomials. Writing $x := \cos\theta$, we use $P_n(x)$ to denote to the n-th Legendre polynomial and $P_n'(x)$ its derivative with respect to x. We look for three solutions of the forms [50]

$$V^+ = \sum_{n=1}^{\infty} c_n \left(\frac{R_m}{r}\right)^{n+2} P_n'(x) \quad P^+ \equiv q_0 \quad r > R_m, \tag{2.12}$$

$$V^- = \sum_{n=1}^{\infty} c_n \left(\frac{r}{R_m}\right)^{n-1} P_n'(x) \quad P^- \equiv q_0 - \frac{2p_0}{R_m} \quad r < R_m, \tag{2.13}$$

$$v = \sum_{n=1}^{\infty} c_n P_n'(x) \quad p \equiv p_0 \quad r = R_m, \tag{2.14}$$

where we accounted for the normal stress jump equation (2.9), the no-slip condition at $r = R_m$ (2.2), and enforced regularity at both $r = 0$ and $r \to \infty$. Note that, in principle, we should have three independent sets of expansion coefficients a_n, b_n and c_n for each of V^+, V^-, v in equations (2.12)–(2.14). However, by the no-slip condition in equation (2.2), all three expansions must coincide when $r = R_m$. Because the P_n' are orthogonal with respect to the inner product,

$$\langle P_n', P_m' \rangle = \int_{-1}^{1} P_n'(x) P_m'(x)(1-x^2)\mathrm{d}x, \tag{2.15}$$

the coefficients of all three expansions must be identical.

The set of coefficients c_n represent the strengths of rotlet moments of progressively higher order (rotlet, rotlet dipole, etc.). To see this, let us consider the first few terms of the expansion (2.12) and list in table 1 (up to multiplicative constants) the corresponding contributions to the external azimuthal flow component $\mathbf{V}^+ \cdot \mathbf{e}_\phi$. Each tabulated singularity is the gradient of the previous one along the z-axis. A pictorial representation of the flows associated with the first three moments is provided in figure 3. Intuitively, the far-field flow outside the membrane is expected to be composed of a contribution from solid-body motion (rotlet), a contribution from the differing rotations of the particle and the fluid membrane due to external drag (rotlet dipole) and higher-order singularities capturing how the drag is distributed on the surface.

We will show in what follows that the total torque on the particle is directly captured by the rotlet strength c_1, as would be expected from physical intuition. To fully characterize the flows, we need to determine the coefficients c_n. With $x = \cos\theta$ and exploiting orthogonality of the Legendre polynomials, the force-balance and no-slip equations (2.10), (2.11) and (2.14) can be expressed as

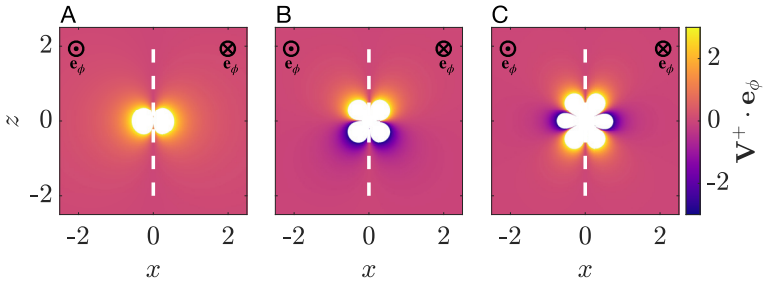

Figure 3. Flows associated with (A) a rotlet, (B) a rotlet dipole, (C) a rotlet quadrupole located at the origin and oriented along the z-axis (dashed white line). In each case, the flow rotates around the z-axis, so a single slice is plotted corresponding to the xz plane. The boundaries of the white patches mark the region where the velocity magnitude (infinite at the origin) first exceeds a set threshold.

Table 1. Velocity field corresponding to each expansion coefficient in equation (2.12). The coefficient c_{n+1} corresponds to a rotlet 2^n-pole, obtained by differentiating the rotlet flow n times with respect to z.

coefficient	velocity	interpretation
c_1	$r^{-2}\sin\theta$	rotlet
c_2	$r^{-3}\sin 2\theta$	rotlet dipole
c_3	$r^{-4}(5\cos^2\theta - 1)\sin\theta$	rotlet quadrupole
⋮	⋮	⋮

(see Appendix C)

$$\frac{(n+1)(n+2)}{(2n+1)(2n+3)}c_{n+1} - \frac{n(n-1)}{(2n-1)(2n+1)}c_{n-1} = \frac{1}{2}\int_{-1}^{1} P_n(x)v(x)(1-x^2)\mathrm{d}x \quad n \geq 0, \tag{2.16}$$

$$(1-x^2)v''(x) - 4xv'(x) = \frac{\varepsilon}{2\theta_p}\sum_{n=1}^{\infty}(2n+1)c_n P_n'(x) \quad x < x_p, \tag{2.17}$$

$$v(x) \equiv \Omega \quad x \geq x_p. \tag{2.18}$$

Here, $x_p = \cos\theta_p$. Furthermore, $\varepsilon = 2\mu R_p/\eta$ is the ratio between the width of the particle, $R_p = R_m\theta_p$, and the Saffman–Delbrück length, $\ell_{\mathrm{SD}} = \eta/\mu$ [31]. The coefficient appearing on the right-hand side of equation (2.17) is thus given by $\varepsilon/2\theta_p = R_m/\ell_{\mathrm{SD}}$, the ratio between the radius of curvature of the membrane and the Saffman–Delbrück length.

Finally, note that the membrane velocity $\mathbf{v}$ has magnitude $\|\mathbf{v}\| = R_m|v|(1-x^2)^{1/2}$. We may thus allow singularities in $v(x)$ at $x = \pm 1$ provided that the velocity is continuous, i.e.

$$v(x)(1-x^2)^{1/2} \quad \text{continuous.} \tag{2.19}$$

Therefore, the flow is fully determined by equations (2.16)–(2.19). These equations also show that the dimensionless flow v/Ω is only a function of two dimensionless parameters, ε and θ_p.

(d) Rotational mobility

The rotational mobility is obtained by computing the total torque $G_p\mathbf{e}_z$ exerted on the particle to maintain the rotation. This torque must balance the drag exerted by the solvents on the top and the bottom of the particle, as well as the in-plane drag on the particle's edge due to the membrane. As shown in Appendix A, however, the total torque on the particle's edge is precisely equal to the

total torque on the membrane with $\theta_p \le \theta \le \pi$. We deduce that G_p must balance the total viscous torque on the particle-membrane assembly caused by the solvents. In other words

$$\begin{aligned} G_p &= -2\pi R_m^3 \int_{-1}^{1} \tau^{\phi}(1-x^2)^{1/2}\mathrm{d}x \\ &= 2\pi\mu R_m^3 \sum_{n=1}^{\infty}(2n+1)c_n \int_{-1}^{1} P_n'(x)(1-x^2)\mathrm{d}x. \end{aligned} \tag{2.20}$$

All terms in the integral above vanish except the first one, leading to

$$G_p = 8\pi\mu c_1 R_m^3, \tag{2.21}$$

and thus all information about the torque is embedded in the rotlet coefficient c_1, as expected. In the rest of the paper, we will write the drag using a standard normalization in terms of the particle radius $R_m\theta_p$ as $G_p \equiv 8\pi\mu\Omega R_m^3\theta_p^3\Lambda_R$, thereby introducing the dimensionless drag coefficient $\Lambda_R(\varepsilon,\theta_p) = \Omega^{-1}\theta_p^{-3}c_1$.

3. Rotational mobilities and membrane flow

The dimensionless drag coefficient Λ_R is a function of two dimensionless parameters: $\varepsilon = 2\mu R_p/\eta$ (ratio of particle size and the Saffman–Delbrück length [27]) and the dimensionless particle half-angle θ_p.

(a) Numerical results

We solve the problem by truncating all sums at $n = k$ for some finite k and then computing the solutions to equations (2.16)–(2.19) semi-analytically. We first solve equation (2.17) for $v(x)$ in terms of the expansion coefficients c_n, and obtain a set of coupled, linear algebraic equations for $c_1, \ldots, c_k$ from equations (2.16) and (2.18). These can then be solved to find c_1, and hence Λ_R (equation (2.21)). Numerically, we see that the number of modes required to attain a given accuracy diverges as $\theta_p \to 0$. We henceforth use $k = 100$ for $\theta_p \ge 0.4$, $k = 200$ for $0.2 \le \theta_p < 0.4$ and $k = 300$ for $\theta_p < 0.2$. These values of k ensure that, in the limit $\eta \to 0$, we recover the mobility of a rotating spherical cap with a relative error no larger than 2% (see §3b(ii)). With the coefficients known, we can evaluate the flow in the membrane and in both solvents, and deduce the rotational mobility of the particle.

We first illustrate in figure 4 the dimensionless magnitude of the membrane velocity, $\|\mathbf{v}\|/R_m\Omega$ and angular velocity $\|\mathbf{v}\|/R_m\Omega\sin\theta$, as well as the dimensionless magnitude of the ambient flows $\|\mathbf{V}^{\pm}\|/R_m\Omega$ for two representative choices of the parameters ε and θ_p: $\varepsilon = 0.05$, $\theta_p = 0.4$ (A–B) and $\varepsilon = 5$, $\theta_p = 1.1$ (C–D). These values were inspired by experiments with phase-separated giant unilamellar vesicles [3]. Taking the representative values $R_p \sim 1$–$10\ \mu$m, $\ell_{SD} \sim 10$–$10^3\ \mu$m [3] provides the estimate $10^{-3} \le \varepsilon \le 10$. In all cases: (i) the particle does rotate like a rigid body, as prescribed (i.e. with constant angular velocity); (ii) the rotational velocity also vanishes at both the north and south pole, as imposed by regularity; and (iii) the external velocity field decays like a rotlet, i.e. as $\mathcal{O}(r^{-2})$. Outside the cap, the velocity profile has an internal maximum when $\varepsilon/2\theta_p = R_m/\ell_{SD} \ll 1$ (i.e. in the limit of a very viscous membrane), by analogy with a rotating solid sphere [32] (figure 4A,B). Mathematically, this limit corresponds e.g. to sending $\eta \to \infty$ for fixed θ_p. Quantitatively, note that sending $\varepsilon/2\theta_p \to 0$ turns (2.17) into

$$(1-x^2)v'' - 4xv' = 0 \tag{3.1}$$

for $-1 \le x \le x_p$, whose only regular solution is $v \equiv \Omega$. In this limit, the flow in figure 4A therefore approaches rigid-body motion, corresponding to a perfect sine wave. This effect is particularly evident in the angular velocity plot, which remains fairly close to 1 throughout. Conversely, when

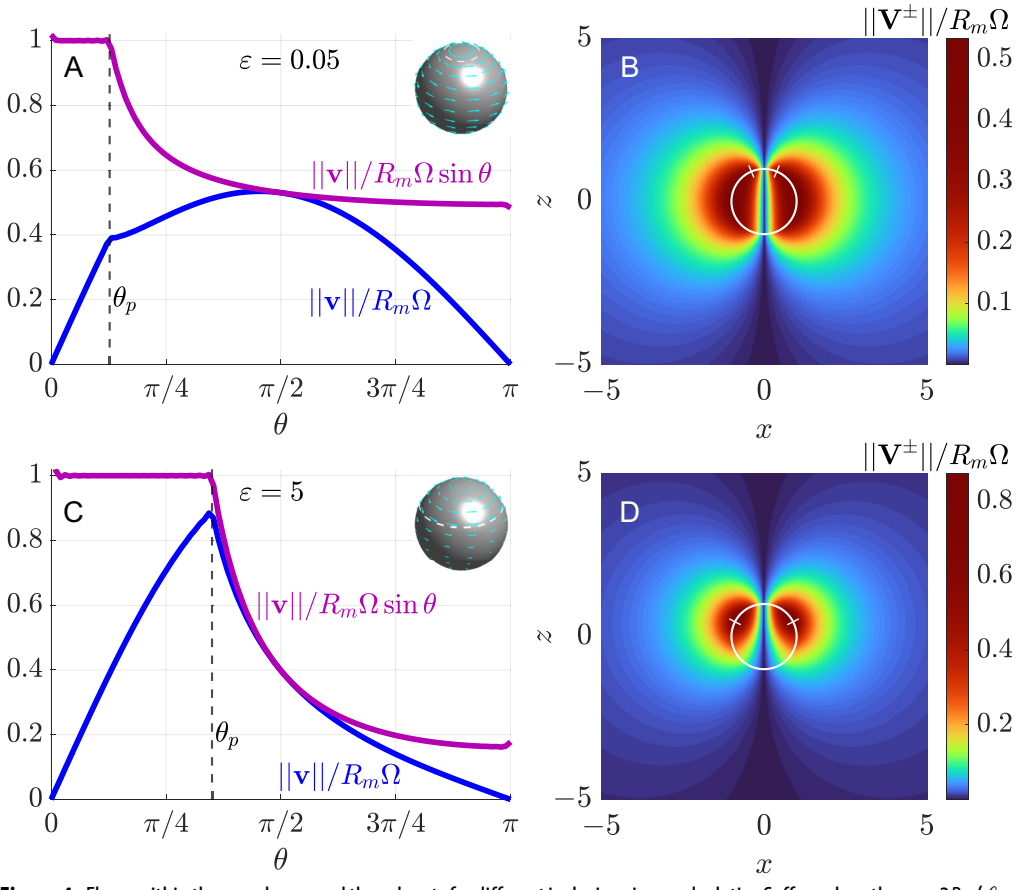

Figure 4. Flows within the membrane and the solvents for different inclusion sizes and relative Saffman lengths $\varepsilon = 2R_p/\ell_{SD}$. (A) Normalized flow in the membrane for $\varepsilon = 0.05$, $\theta_p = 0.4$ (blue line) and its relative solid-body motion component (purple line). Inset: three-dimensional plot of the membrane velocity field. (B) Illustration of solvent flow (iso-magnitude) for the same values of ε, θ_p as (A); since the setup has rotational symmetry, we only plot the magnitude of the azimuthal flow component of the ambient flows in the plane $y = 0$. The white circles represent the membrane, with radial ticks marking the particle edge. (C), (D) Same as (A), (B) with parameters $\varepsilon = 5$, $\theta_p = 1.1$.

$\varepsilon/2\theta_p \gtrsim \mathcal{O}(1)$, the membrane flow is seen to decay monotonically (figure 4C,D), and the angular velocity is substantially smaller than for rigid-body motion.

Next, we study the dependence of the torque exerted on the particle on the two relevant dimensionless parameters, ε and θ_p. The results are displayed in figure 5A, where we plot the torque G_p applied on the particle to maintain the rotation as a function of the particle half-angle θ_p, non-dimensionalized by the torque G_m exerted on a rigid sphere of radius R_m rotating with the same angular velocity. The chosen parameter values, $\theta_p \geq 0.1$ and $0.1 \leq \varepsilon \leq 100$, correspond to a membrane viscosity of 10^{-10} Nsm$^{-1} \lesssim \eta \lesssim 10^{-6}$ Nsm^{-1} for a 50 µm vesicle, a range covering typical values for giant unilamellar vesicles [3].

As expected, the normalized torque $G_p/G_m \to 1$ as $\theta_p \to \pi$ since, in this limit, the particle covers the entirety of the vesicle, making the membrane completely rigid. Conversely, the torque vanishes for a small particle ($\theta_p \to 0$). For a given particle size and solvent viscosities, the applied torque increases with the Saffman–Delbrück length ℓ_{SD}, as a larger ℓ_{SD} corresponds to a more viscous, and hence more rigid, membrane. This effect is more obvious for larger values of θ_p as the membrane's angular velocity, which is nearly constant due to the small azimuthal shear, has less room to vary. Finally, in figure 5B we explore a different definition of particle

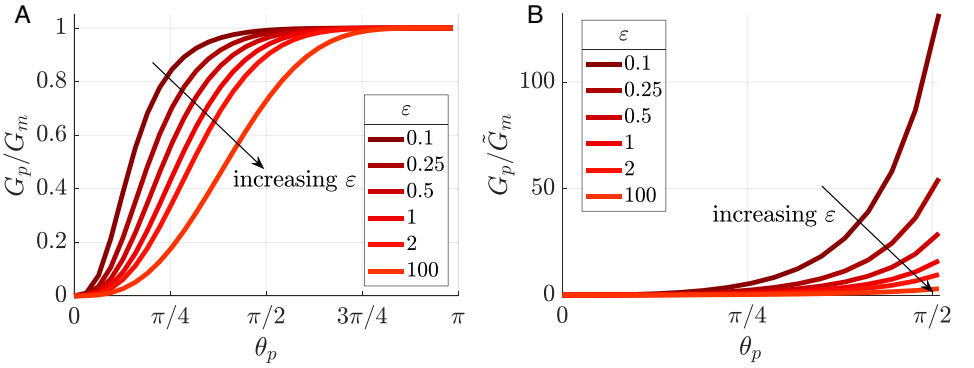

Figure 5. Dependence of the exerted torque on the particle size and the membrane viscosity: (A) torque G_p exerted on the particle to maintain rotation (non-dimensionalized by the torque G_m on a rigid sphere of radius R_m rotating with the same angular velocity in a solvent with viscosity μ) as a function of the half-angle θ_p of the particle, for a range of values of the modified viscosity ratio $\varepsilon = 2\mu R_p/\eta = 2R_p/\ell_{SD}$. For a fixed particle size, the torque increases for larger ℓ_{SD} (i.e. for decreasing ε). (B) Torque G_p exerted on the particle to maintain rotation non-dimensionalized by the torque $\tilde{G}_m$ exerted on a rigid sphere (radius R_m, ambient viscosity μ) rotating at the modified rate $\Omega - c_1$ (i.e. the difference between Ω and the rigid motion of the membrane).

mobility [19], defined in the frame co-rotating with the rigid-body motion of the membrane. In particular, we plot the torque on the inclusion non-dimensionalized by the torque $\tilde{G}_m$ on a rigid sphere (radius R_m) rotating with angular velocity $\Omega - c_1$ in the same solvents, where c_1 corresponds to the membrane's solid-body motion. The ratio $G_p/\tilde{G}_m$ is larger when the membrane is more viscous (smaller ε), as this impedes differential rotation between the membrane and the particle. The relative torque in figure 5B also blows up for large inclusions ($\theta \to \pi$) as shearing the membrane becomes increasingly hard. A co-rotating drag coefficient may then be defined as $\tilde{\Lambda}_R = (\Omega - c_1)^{-1}\theta_p^{-3}c_1$. In terms of the free mobility, $\tilde{\Lambda}_R = (1 - c_1/\Omega)^{-1}\Lambda_R$, implying that the two coefficients differ when the solid-body rotation of the membrane is significant (i.e. for sufficiently large ℓ_{SD} or large inclusions).

(b) Asymptotic results

Our setup contains three inherent length scales, namely the curvilinear particle radius R_p, the membrane radius R_m and the Saffman–Delbrück length ℓ_{SD}, with corresponding dimensionless ratios $R_p/R_m = \theta_p$ and $\ell_{SD}/R_m = 2\theta_p/\varepsilon$. To understand the interactions between the various length scales, we now analyse two asymptotic limits, with results summarized in figure 6. First, in §3b(i), we consider the limit of a small particle ($R_p/R_m \ll 1$ or $\theta_p \ll 1$) of varying Saffman–Delbrück length, or equivalently of varying ε. In this case, we observe a transition from planar mobility [31] to spherical mobility as the membrane becomes more and more viscous ($\ell_{SD} \to \infty$). We then address the limit of a particle of size comparable with the membrane, i.e. $R_p \sim R_m$ (§3b(ii)); we demonstrate that, in the limit of small Saffman–Delbrück length ($\ell_{SD} \ll R_p$ or $\varepsilon \gg 1$), the hydrodynamic effects of the membrane are negligible and the particle experiences the same drag as a rotating spherical cap in an unbounded fluid [51]. As the Saffman length increases, the torque instead becomes the same as on a rotating rigid sphere (see figure 5).

(i) Small particle limit: $R_p/R_m \ll 1$

Firstly, we consider a particle that is much smaller than the membrane and compare the numerically calculated mobility with the planar value [31]. Experimentally, this limit is appropriate for smaller inclusions, such as membrane-bound proteins and microspheres [18]. It is

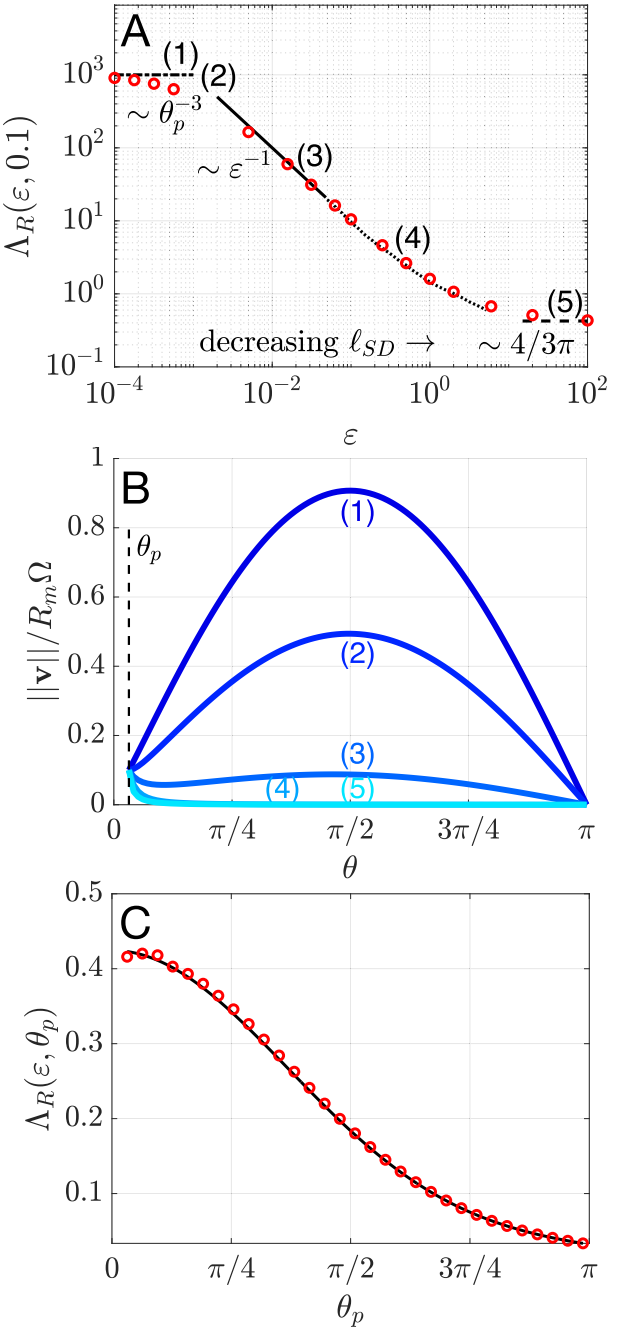

Figure 6. Asymptotic behaviour of rotational drag coefficient, $\Lambda_R(\varepsilon, \theta_p)$, in the limits of small and large particles. (A) Small particle limit, $R_p \ll R_m$ (or $\theta_p \ll 1$) for many values of $\varepsilon = 2R_p/\ell_{SD}$ (numerics run with $\theta_p = 0.1$, $k = 300$), with details in §3b(i). The numerical values of Λ_R (red circles) are compared with (1) the solid-body motion limit $\Lambda_R \sim \theta_p^{-3}$, (3) the asymptotic behaviour $\Lambda_R \sim \varepsilon^{-1}$ (solid black line), (4) the analytical prediction from figure 3 in [31] (dotted black line) and (5) the asymptotic behaviour $\Lambda_R \sim 4/3\pi$ for a rotating disc [28] (dashed black line). Region (2) marks the transition between the three-dimensional mobility in (1) and the nearly planar mobility in (3). (B) Plot of the dimensionless membrane velocity ($\theta \geq \theta_p$) for a small particle ($\theta_p = 0.1$) and representative values of ε for each region: (1) $\varepsilon = 10^{-4}$, (2) $\varepsilon = 10^{-3}$, (3) $\varepsilon = 10^{-2}$, (4) $\varepsilon = 2$, (5) $\varepsilon = 20$. (C) Small Saffman–Delbrück length limit, $\ell_{SD} \ll R_p \sim R_m$ (or $\theta_p/\varepsilon \ll \theta_p$, 1), with details in §3b(ii). Numerical results ($0.1 \leq \theta_p \leq 3.1$ and $\varepsilon = 200$, red circles) are compared with the analytical solution for a spherical cap (solid black line) [51].

common in the literature to infer the membrane's viscosity by measuring the diffusion coefficient of such inclusions and relating it to the viscosity as in Saffman's planar theory [15,29]. We will show below that, in the rotational case, such approximation is appropriate as long as η is not too large. As the Saffman–Delbrück length is varied from small values (highly viscous solvents) to large values (highly viscous membrane), five distinct asymptotic regions emerge (figure 6A), which we set out to explain below.

Rigid rotation (1) When ℓ_{SD} is large (figure 6A, region (1)), the membrane rotates rigidly to minimize dissipation (figure 5) [27,32]. The torque on the cap is therefore approximately $8\pi\mu\Omega R_m^3$, and therefore $\Lambda_R \sim \theta_p^{-3}$. This regime occurs when the torque associated with rigid rotation of the whole vesicle is much less than the torque associated with non-zero membrane shear. Importantly, this regime is not captured by the planar Saffman theory, which assumes the membrane to be at rest far from the inclusion.

Transition (2) and two-dimensional limit (3) As the Saffman–Delbrück length is reduced, the membrane begins to experience shear from the particle. For $\ell_{SD} \gg R_p$, the drag from the solvents is negligible on the scale of the particle and the local flow is purely two-dimensional [49]. The particle mobility is in this case $\Lambda_R \sim \varepsilon^{-1}$, the same as a disc in an infinite two-dimensional fluid without any solvents, a problem that is not subject to Stokes paradox (figure 6A, region (3)) [28,29,31]. The transition region (2) between the previous two regimes therefore occurs when $\varepsilon^{-1} \sim \theta_p^{-3}$, signifying that regime (1) corresponds to $\varepsilon \ll \theta_p^3$, or equivalently $\ell_{SD} \gg R_m^3/R_p^2$. Region (3) instead corresponds to $\theta_p^3 \ll \varepsilon \ll 1$, or $R_p \ll \ell_{SD} \ll R_m^3/R_p^2$. Region (2) is physically significant as the inclusion ceases to feel the effect of the membrane's geometry (dominant in (1)) and the flow becomes local, rendering the mobility nearly planar (region (3)).

The asymptotic behaviour in region (3), corresponding to $\theta_p^3 \ll \varepsilon \ll 1$ or $R_p \ll \ell_{SD} \ll R_m^3/R_p^2$, can be recovered mathematically by noting that the local flow varies on the length scale of the particle [32], since the solvents are negligible within a distance $\mathcal{O}(\ell_{SD})$ of the particle. Therefore, the torque is caused predominantly by the in-plane membrane shear, implying that

$$\Lambda_R \sim \frac{1}{8\pi\mu\Omega R_m^3\theta_p^3}\int_{\phi=0}^{2\pi} R_m^2 \mathbf{e}_r \times \boldsymbol{\sigma}\cdot\mathbf{e}_\theta \sin\theta_p \mathrm{d}\phi = \frac{v'(x_p)(1-x_p^2)^2}{2\varepsilon\theta_p^2\Omega}. \tag{3.2}$$

To proceed, we need to determine v around the particle. Since the flow varies on an angle θ_p, by locally writing $x = 1-\theta_p^2 X$ with $X = \mathcal{O}(1)$, from equation (2.17)

$$\begin{aligned} &(1-x^2)v''(x) - 4xv'(x) = \mathcal{O}(R_m v/\ell_{SD}) \\ \Rightarrow\ &Xv''(X) + 2v'(X) = \mathcal{O}(R_p^2 v/R_m\ell_{SD}) \sim 0 \\ \Rightarrow\ &v = \frac{A}{X} + B, \end{aligned} \tag{3.3}$$

where in (equation (3.3)) we exploited the fact that $R_p^2 v/\ell_{SD}R_m \ll v$. Notice that the torque associated with the solid-body motion B is $\sim \mu B R_m^3$, while the torque on the particle is $G_p \sim \eta R_p^2 v$. Equating these, we obtain $B \sim \ell_{SD}R_p^2 v/R_m^3$, which is much less than v in region (3). Setting $B = 0$ at leading order, the boundary conditions are $v = \Omega$ on $x = 1-\theta_p^2/2 + \mathcal{O}(\theta_p^4)$, i.e. $v(X = 1/2) = \Omega$. This yields $A = \Omega/2$, giving the inner solution

$$v = \frac{\Omega}{2X} = \frac{\Omega(1-x_p^2)}{2(1-x)}. \tag{3.4}$$

This is indeed analogous to the flow around a spinning cylinder in a flat, solvent-free membrane ($v \sim d^{-2}$ with $d = \sin\theta/\sin\theta_p$). We deduce that, as $x_p \to 1$,

$$v'(x_p)(1-x_p^2) \approx \frac{1}{2}\Omega(1+x_p)^2 \approx 2\Omega, \tag{3.5}$$

Table 2. The drag coefficient (Λ_R) of a small particle ($R_p/R_m \ll 1$) as the Saffman length ℓ_{SD} is varied shows five different asymptotic behaviours. Investigation of the limits $\ell_{SD} \gg R_m^3/R_p^2$, $\ell_{SD} \sim R_m^3/R_p^2$ and $\ell_{SD} = \mathcal{O}(R_p)$ represents an extension of the results in [18] for a point-like particle ($R_p = 0$).

asymptotic limit	drag coefficient	refs	interpretation
$\ell_{SD} \gg R_m^3/R_p^2$	$\Lambda_R \sim (R_m/R_p)^3$	[52,53]	solid-body membrane rotation
$\ell_{SD} \sim R_m^3/R_p^2$	$\Lambda_R \sim (R_m/R_p)^3$	[52,53]	near-rigid membrane rotation with small shear
$R_p \ll \ell_{SD} \ll R_m^3/R_p^2$	$\Lambda_R \sim \ell_{SD}/2R_p$	[15]	cylinder in two-dimensional fluid (no solvents)
$\ell_{SD} \sim R_p$	$\Lambda_R = \mathcal{O}(1)$	[31]	cylinder in two-dimensional fluid with solvents
$\ell_{SD} \ll R_p$	$\Lambda_R \sim 4/3\pi$	[28]	disc in three-dimensional fluid

and therefore the dimensionless friction coefficient is

$$\Rightarrow \Lambda_R \sim \varepsilon^{-1}, \tag{3.6}$$

as observed in figure 6A.

Planar regime (4) As the membrane viscosity is reduced further, eventually $\varepsilon \sim 1$ or $\ell_{SD} \sim R_p$ (figure 6A, region (4)). In this regime the mobility is asymptotically the same as in the planar regime with contributions to the drag from both the membrane and the solvents [31], as the small particle is oblivious to the membrane's geometry.

Solvent-dominated limit (5) Finally, when the membrane viscosity is very low ($\varepsilon \gg 1$ or $\ell_{SD} \ll R_p$), we observe one more regime (figure 6A, region (5)) where the membrane virtually disappears and Λ_R is the same as the three-dimensional mobility of a disc in the solvent, namely $\Lambda_R \sim 4/3\pi$ [28].

A summary of the identified asymptotic limits is provided in table 2. An implication of our analysis is that the planar Saffman theory therefore captures the mobility of small inclusions as long as ℓ_{SD} is not too large, specifically $\ell_{SD} \ll R_m^3/R_p^2$. We also note that the asymptotic behaviour in region (5), corresponding to $\varepsilon \gg 1$ or $\ell_{SD} \ll R_p$ is a reflection of the spherical geometry of our setup. Indeed, while it is evident from equation (2.7) that the membrane applies negligibly small in-plane stresses on the solvents, in-plane membrane incompressibility in general poses a non-trivial constraint on the ambient flows due to the no-slip condition. It is for instance well-known that a flat membrane with asymptotically small viscosity affects the leading-order translational resistance of a particle [31]. In a spherical geometry, on the other hand, any purely azimuthal surface flow is automatically divergence-free, so membrane incompressibility does not constrain solvent flow and the limit $\eta \to 0$ is regular (i.e. the membrane simply disappears).

The membrane flow is qualitatively different in regions (1)–(5). As shown in figure 6B, for values of ε in region (1), the membrane essentially rotates rigidly to reduce in-plane shear. This effect lingers in region (2), but the increased shear noticeably slows down rotation. In region (3), corresponding to $\theta_p^3 \ll \varepsilon \ll 1$, the membrane transitions from the high curvature regime, $R_m \ll \ell_{SD}$ ($\varepsilon \ll \theta_p$), to the low curvature regime, $R_m \gg \ell_{SD}$ ($\varepsilon \gg \theta_p$). Interestingly, this transition is associated with a loss of monotonicity and the creation of an internal minimum near the inclusion [32], while rotation near the equator is nearly rigid to reduce the otherwise large in-plane shear. Finally, as the membrane viscosity is reduced further, the membrane flow decreases monotonically on the length scale of the particle with minimal qualitative differences between regions (4) and (5).

(ii) Large particle limit: $R_p \sim R_m$

We now consider the case of particle of size comparable with that of the membrane, similar to experimental observations of liquid domains in phase-separated giant unilamellar vesicles

[3]. As already shown in figure 5 and in §3b(i), when the membrane is very viscous ($\ell_{SD}/R_p \sim \ell_{SD}/R_m \gg 1$), the system rotates rigidly and $\Lambda_R \sim \theta_p^{-3}$. In this section, we investigate the opposite limit of a nearly inviscid membrane ($\ell_{SD}/R_p \sim \ell_{SD}/R_m \ll 1$). As explained in §3b(i), the membrane effectively disappears for small ℓ_{SD}. It is therefore natural to compare our numerical results for Λ_R with the exact rotational mobility of a spherical cap $\hat{\Lambda}_R$ obtained in the absence of a membrane [51]

$$\hat{\Lambda}_R(\theta_p) = \frac{1}{8\pi\theta_p^3}\left(8\theta_p - 4\sin 2\theta_p + \frac{16}{3}\sin^3\theta_p\right). \tag{3.7}$$

Consistently with the aforementioned result for a rotating disc in an unbounded fluid [28], we have $\hat{\Lambda}_R \to 4/3\pi$ as $\theta_p \to 0$, while $\hat{\Lambda}_R \to \theta_p^{-3}$ when $\theta_p \to \pi$ (i.e. the particle becomes a spherical shell). We compare the limit in equation (3.7) with our numerical results in figure 6C. We see that very good agreement is obtained throughout the domain, confirming that the membrane indeed vanishes as $\eta \to 0$.

4. Conclusion

In this paper, we computed the rotational mobility of a rigid particle embedded inside a spherical membrane for various particle sizes and Saffman–Delbrück length scales. The calculation was motivated by a number of relevant biological situations, such as the movement of ATP synthase [45], aquaporin channels [9–11] and the Brownian motion of membrane-embedded particles [46]. We started with the most general force-balance equations for the membrane and eventually obtained an ODE for the membrane flow $\mathbf{v}$. After expanding the ambient and membrane flows with respect to a polynomial basis, we reduced the problem to an infinite set of linear equations depending only on two dimensionless parameters: ε and θ_p. These correspond to $\varepsilon = 2\mu R_p/\eta = 2R_p/\ell_{SD}$, the ratio of the curvilinear particle radius and the Saffman–Delbrück length, and $\theta_p = R_p/R_m$, the half-angle of the particle. Using a truncation to a finite number of modes, the resulting system could be solved semi-analytically, allowing us to compute the dimensionless rotational resistance Λ_R for many values of ε and θ_p, with results summarized in figure 5. We then explored the physical significance of the three relevant length scales—curvilinear particle radius R_p, Saffman–Delbrück length ℓ_{SD}, and membrane radius R_m—by considering different asymptotic limits. We demonstrated that the particle only sees the spherical geometry of the membrane when $R_p = \mathcal{O}(R_m)$ or when the membrane viscosity is sufficiently high, while for sufficiently small $R_p \ll R_m$ the flow is purely local and the mobility is set by the planar limit [31]. The Saffman–Delbrück length operates as a cut-off length beyond which the flow is affected by the solvent traction. In particular, for small ℓ_{SD} the membrane disappeared altogether, while for large ℓ_{SD} the membrane rotated almost rigidly as if the solvents were not present.

From a theoretical standpoint, this work sheds light on the interplay between particle geometry and intrinsic length scales in determining local flow and particle mobility. This is made possible by considering a finite-sized particle, rather than a point-like inclusion [32]. Computationally, we were able to numerically recover past results for planar mobility and the torque on a spherical cap as special cases of our geometry [29,31,51]. The numerical implementation of a spherical membrane of vanishing viscosity (a limit which we showed to be regular unlike in the planar case [31]) may prove a valuable computational tool when dealing with rotational flow with spherical geometries.

Biologically, our work provides a way of estimating the viscosity of membranes containing large inclusions [3], which are affected by the membrane's geometry. Current experimental measurements of η typically approximate the membrane as planar [18] and rely on Saffman's theory to estimate η from the translational diffusion coefficient [15,29,31] of membrane-bound proteins and microspheres [47]. When the inclusion is too large for Saffman's theory to apply, such as for large proteins [36,42], our work suggests that one may instead measure the rotational diffusion coefficient D_R of the inclusion and exploit Einstein's relation $D_R = k_B T/G_p$ [15] to determine the torque, $G_p = k_B T/D_R$. Our predictions in figure 5 may then be used to estimate

ε, and thus η. It should however be noted that measuring the rotational mobility may pose a significant challenge, requiring the invention of bespoke experimental protocols.

An important extension of this work will consist of studying the other relevant mobility component, namely the translational mobility of the particle. This is expected to be significantly more challenging, as the resulting physical system will no longer be rotationally symmetric. It may likewise be physically relevant to analyse the case of a non-circular particle [44]. Furthermore, one could allow the interior and exterior solvents to have different viscosities, as may be the case for cells whose cytoplasm viscosity is larger than that in the surroundings. Other directions for future work include the interactions of multiple rotating particles, or adapting the theory to the case of non-rigid inclusions, such as liquid domains [3]. The rotational diffusion of liquid domains arises as a result of random molecular torques [15]. Such torques are applied on extremely fast timescales, giving rise to oscillatory flows within the domain and the membrane. An unsteady version of our theory will therefore be needed to capture this effect [52,53]. It may also be biologically relevant [20] to allow for a more realistic membrane rheology, including viscoelastic effects [12,54].

Data accessibility. The codes used to perform the numerical calculations as well as to generate the figures are accessible via the following link: https://github.com/MarcoVona99/Large_Inclusion_Mobility.

Declaration of AI use. We have not used AI-assisted technologies in creating this article.

Authors' contributions. M.V.: methodology, writing—original draft; E.L.: supervision, writing—review and editing.

Both authors gave final approval for publication and agreed to be held accountable for the work performed therein.

Conflict of interest declaration. We declare we have no competing interests.

Funding. This work was funded in part by EPSRC (scholarship to MV).

Appendix A. Force and torque balance equations in the membrane

For the purposes of obtaining a general theory, let the membrane be parametrized by arbitrary curvilinear coordinates $(x^1, x^2) \in \Sigma \subseteq \mathbb{R}^2$. Taking $\mathbf{r}$ to be the position vector in $\mathbb{R}^3$, we may endow the membrane with a coordinate basis $\mathbf{e}_a = \mathbf{r}_{,a}$. We further denote the unit normal to the membrane by $\mathbf{n}$, the metric tensor by $g_{ab} = \mathbf{e}_a \cdot \mathbf{e}_b$ and the extrinsic curvature tensor by $K_{ab} = \mathbf{n} \cdot \partial_b \mathbf{e}_a$. The viscous stresses in the membrane are described by a stress tensor σ^{ab}, such that the force $\mathbf{f}$ per unit length on a curve with unit normal $\mathbf{p}$ (tangent to the membrane) is $\mathbf{f} = \sigma^{ab} p_a \mathbf{e}_b$. Apply the force-balance condition to a small area patch $\mathcal{A}$ with boundary $\partial\mathcal{A}$ and local boundary unit normal p_a (figure 7). The external viscous force on this patch is $\mathbf{T}\|\mathcal{A}\| + \mathcal{O}(\|\mathcal{A}\|^2)$, where the norm denotes the area. By the standard divergence theorem in $\mathbb{R}^2$, letting $g = \det(g_{ab})$, the viscous force due to stresses in the membrane is

$$\oint_{\partial\mathcal{A}} \sigma^{ab} \boldsymbol{e}_b p_a \mathrm{d}s = \int_{\Sigma} \partial_a \left(\sigma^{ab} \boldsymbol{e}_b \sqrt{g}\right) \mathrm{d}x^1 \mathrm{d}x^2 \tag{A 1}$$

$$= \int_{\mathcal{A}} \frac{1}{\sqrt{g}} \partial_a \left(\sigma^{ab} \boldsymbol{e}_b \sqrt{g}\right) \mathrm{d}S = \frac{1}{\sqrt{g}} \partial_a \left(\sigma^{ab} \boldsymbol{e}_b \sqrt{g}\right) \|\mathcal{A}\| + \mathcal{O}\left(\|\mathcal{A}\|^2\right). \tag{A 2}$$

Assuming the membrane is viscous enough for inertia to be negligible, forces must locally balance. As a result, for $\|\mathcal{A}\| \to 0$,

$$\frac{1}{\sqrt{g}} \partial_a \left(\sigma^{ab} \boldsymbol{e}_b \sqrt{g}\right) + \mathbf{T} = \mathbf{0} \tag{A 3}$$

$$\Rightarrow (\partial_a \sigma^{ab} + \Gamma^c_{ac} \sigma^{ab} + \Gamma^b_{ac} \sigma^{ac}) \mathbf{e}_b + \sigma^{ab} K_{ab} \mathbf{n} + \mathbf{T} = \mathbf{0} \tag{A 4}$$

$$\Rightarrow (\nabla_a \sigma^{ab}) \mathbf{e}_b + \sigma^{ab} K_{ab} \mathbf{n} + \mathbf{T} = \mathbf{0}, \tag{A 5}$$

where we exploited the fact that $\partial_a \sqrt{g} = \Gamma^b_{ab} \sqrt{g}$ in equation (A 4). The expression in equation (A 5) is now equal to equation (2.7) in the main body of the paper. An equivalent way to express

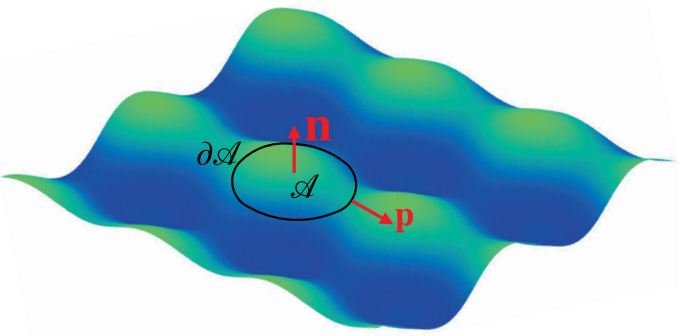

Figure 7. Force balance sketch: the membrane viscous forces exerted on the boundary of the area patch $\mathcal{A}$ with unit normal $\mathbf{n}$, boundary $\partial\mathcal{A}$ and boundary unit normal $\mathbf{p}$ should balance the viscous forces generated by the solvents. Exploiting the arbitrariness of $\mathcal{A}$ yields the membrane Stokes (2.7).

force balance, more reminiscent of the standard Stokes equations, is obtained by rewriting equation (A 3) as

$$\mathrm{div}_s(\sigma^{ab}\mathbf{e}_a \otimes \boldsymbol{e}_b) + \mathbf{T} = \mathbf{0}, \tag{A 6}$$

where the operator $\mathrm{div}_s = \mathbf{e}^a\partial_a$ denotes the surface divergence [22]. To see why (not to be confused with the covariant derivative). To see why equation (A 6) holds, note that from the Leibniz rule for partial derivatives we have

$$\mathbf{e}^c\partial_c(\sigma^{ab}\mathbf{e}_a \otimes \boldsymbol{e}_b) = (\nabla_c\sigma^{ab})\mathbf{e}^c \otimes \mathbf{e}_a \otimes \mathbf{e}_b + \sigma^{ab}\mathbf{e}^c \otimes (K_{ac}\mathbf{n}) \otimes \mathbf{e}_b + \sigma^{ab}\mathbf{e}^c \otimes \mathbf{e}_a \otimes (K_{bc}\mathbf{n}), \tag{A 7}$$

and therefore, contracting the first tensor product

$$\mathrm{div}_s(\sigma^{ab}\mathbf{e}_a \otimes \boldsymbol{e}_b) = (\nabla_a\sigma^{ab})\mathbf{e}_b + \sigma^{ab}K_{ab}\mathbf{n}. \tag{A 8}$$

Finally, integrating equation (A 6) over the membrane, we obtain that the total external force $\int_{\mathcal{M}}\mathbf{T}\mathrm{d}S$ reduces to a boundary term, and hence vanishes for a closed membrane with no inclusions. By a similar argument as for the forces, torques balance within the membrane, as for any area patch $\mathcal{B}$

$$\begin{aligned}\int_{\partial\mathcal{B}}\mathbf{r}\times\sigma^{ab}\mathbf{e}_b p_a\mathrm{d}s &= \int_{\mathcal{B}}\partial_a(\mathbf{r}\times\sigma^{ab}\mathbf{e}_b\sqrt{g})\mathrm{d}x^1\mathrm{d}x^2\\ &= \int_{\mathcal{B}}\sigma^{ab}\mathbf{e}_a\times\mathbf{e}_b\sqrt{g}\mathrm{d}x^1\mathrm{d}x^2 + \int_{\mathcal{B}}\mathbf{r}\times\frac{1}{\sqrt{g}}\partial_a(\sigma^{ab}\mathbf{e}_b\sqrt{g})\mathrm{d}S. \qquad \text{(A 9)}\\ &= \int_{\mathcal{B}}\mathbf{r}\times\mathrm{div}_s(\sigma^{ab}\mathbf{e}_a\otimes\mathbf{e}_b)\mathrm{d}S\\ &= \int_{\mathcal{B}}-\mathbf{r}\times\mathbf{T}\mathrm{d}S. \qquad \text{(A 10)}\end{aligned}$$

Note that in equation (A 9) we have used the identity $\mathbf{r}_{,a} = \mathbf{e}_a$ and the first integral cancels due to symmetry of σ^{ab}. For our problem, this means that the total torque on the particle is equal to the torque on the membrane-particle system from the external solvent.

Appendix B. Membrane flow equation as limit of the three-dimensional Stokes equations

To further elucidate the two-dimensional flow model for the membrane, in this Appendix we derive (2.10) as the limit of the standard three-dimensional Stokes equations.

We start by approximating the membrane as a thin layer of Newtonian fluid in a spherical annulus $R_m \le r \le R_m + \Delta R_m$ with viscosity $\overline{\eta}$. Because of the presence of undeformable molecules oriented normal to the membrane [17], we assume that such a fluid layer must have vanishing radial shear; using $\mathbf{E}$ to denote the rate-of-strain tensor, this means that $\mathbf{E}_{rr} = \mathbf{E}_{r\theta} = \mathbf{E}_{r\phi} = 0$. In a rotationally symmetric setup, this constrains the flow to be of the form

$$\mathbf{u} = rv(\theta)\sin\theta\mathbf{e}_\phi, \quad R_m \le r \le R_m + \Delta R_m. \tag{B 1}$$

Flow in the membrane is affected by the traction from the solvents, which can be thought of as a force per unit volume $f\boldsymbol{\phi}$. The corresponding forced three-dimensional membrane Stokes equation $\nabla\overline{p} - \overline{\eta}\nabla^2\mathbf{u} = f\mathbf{e}_\phi$ is now

$$\overline{\eta}\,(v''\sin\theta + 3v'\cos\theta) + rf = 0. \tag{B 2}$$

In the limit of a thin membrane with $\Delta R_m/R_m \ll 1$, the total force on a volume element should be the same as the traction on the upper and lower surfaces, i.e.

$$f\Delta R_m = \tau^\phi. \tag{B 3}$$

Assuming a very viscous membrane, sending now $\Delta R_m \to 0$, so that $r \to R_m$, while keeping the effective two-dimensional membrane viscosity $\eta = \overline{\eta}\Delta R_m$ constant leads to

$$\eta(v''\sin\theta + 3v'\cos\theta) + R_m\tau^\phi = 0. \tag{B 4}$$

This coincides with (2.10) in the main text, showing that the previously introduced two-dimensional model of the membrane is obtained as the limit of a thin, non-shearing three-dimensional flow.

Appendix C. Derivation of governing equations (2.16) and (2.17)

In order to determine the flow in the membrane and the solvents, we need to find the expansion coefficients c_n. These can be expressed in terms of $v(x)$ by multiplying (2.14) by $1 - x^2$ and taking the inner product with P_m. Using the classical equalities [55,56]

$$(1-x^2)P_n' = n(P_{n-1} - xP_n), \tag{C 1}$$

$$\int_{-1}^{1} P_n(x)P_m(x)\mathrm{d}x = \frac{2\delta_{n,m}}{2n+1}, \tag{C 2}$$

$$\int_{-1}^{1} xP_n(x)P_m(x)\mathrm{d}x = \frac{2(m+1)}{(2m+1)(2m+3)}\delta_{n,m+1} + \frac{2m}{(2m-1)(2m+1)}\delta_{n,m-1}, \tag{C 3}$$

$$\tag{C 4}$$

for $n, m \ge 0$, we readily obtain the recursive relationship for $n \ge 0$

$$\frac{(n+1)(n+2)}{(2n+1)(2n+3)}c_{n+1} - \frac{n(n-1)}{(2n-1)(2n+1)}c_{n-1} = \frac{1}{2}\int_{-1}^{1} P_n(x)v(x)(1-x^2)\mathrm{d}x. \tag{C 5}$$

The membrane velocity $v(x)$ and the coefficients c_n are also coupled via the momentum equation (2.10). Substituting $x = \cos\theta$, this takes the form

$$\eta[(1-x^2)v''(x) - 4xv'(x)] + R_m(1-x^2)^{-1/2}\tau^\phi = 0 \quad \theta_p < \theta \le \pi \text{ (membrane)}. \tag{C 6}$$

The azimuthal tractions may be evaluated as

$$(1-x^2)^{-1/2}\tau^\phi = \mu R_m\left[\frac{\partial(V_+^\phi - V_-^\phi)}{\partial r}\right]_{r=R_m} = -\mu\sum_{n=1}^{\infty}(2n+1)c_nP_n'(x), \tag{C 7}$$

finally yielding

$$(1-x^2)v''(x) - 4xv'(x) = \frac{\mu R_m}{\eta}\sum_{n=1}^{\infty}(2n+1)c_n P_n'(x) = 0 \quad x \geq x_p \text{ (membrane)}, \tag{C 8}$$

which is the same as (2.17) in the main text.

References

1. Veatch SL, Keller SL. 2005 Miscibility phase diagrams of giant vesicles containing sphingomyelin. *Phys. Rev. Lett*. **94**, 148101. (doi:10.1103/physrevlett.94.148101)
2. Veatch SL, Keller SL. 2005 Seeing spots: complex phase behavior in simple membranes. *BBA Mol. Cell Res*. **1746**, 172–185. (doi:10.1016/j.bbamcr.2005.06.010)
3. Cicuta P, Keller SL, Veatch SL. 2007 Diffusion of liquid domains in lipid bilayer membranes. *J. Phys. Chem. B* **111**, 3328–3331. (doi:10.1021/jp0702088)
4. Dinsmore AD, Hsu MF, Nikolaides MG, Marquez M, Bausch AR, Weitz DA. 2002 Colloidosomes: selectively permeable capsules composed of colloidal particles. *Science* **298**, 1006–1009. (doi:10.1126/science.1074868)
5. Maier B, Rädler JO. 2000 DNA on fluid membranes: a model polymer in two dimensions. *Macromolecules* **33**, 7185–7194. (doi:10.1021/ma000075n)
6. Stone HA, Ajdari A. 1998 Hydrodynamics of particles embedded in a flat surfactant layer overlying a subphase of finite depth. *J. Fluid Mech*. **369**, 151–173. (doi:10.1017/s0022112098001980)
7. McConnell HM. 1991 Structures and transitions in lipid monolayers at the air-water interface. *Annu. Rev. Phys. Chem*. **42**, 171–195. (doi:10.1146/annurev.pc.42.100191.001131)
8. Spooner PJR, Friesen RHE, Knol J, Poolman B, Watts A. 2000 Rotational mobility and orientational stability of a transport protein in lipid membranes. *Biophys. J*. **79**, 756–766. (doi:10.1016/s0006-3495(00)76333-8)
9. Gravelle S, Joly L, Detcheverry F, Bocquet L. 2013 Optimizing water permeability through the hourglass shape of aquaporins. *Proc. Natl. Acad. Sci*. **110**, 16367–16372. (doi:10.1073/pnas.1306447110)
10. de Groot BL, Grubmüller H. 2001 Water Permeation Across Biological Membranes: Mechanism and Dynamics of Aquaporin-1 and GlpF. *Science* **294**, 2353–2357. (doi:10.1126/science.1066115)
11. Gonen T, Walz T. 2006 The structure of aquaporins. *Q. Rev. Biophys*. **39**, 361–396. (doi:10.1017/s0033583506004458)
12. Rahimi M, DeSimone A, Arroyo M. 2013 Curved fluid membranes behave laterally as effective viscoelastic media. *Soft Matter* **9**, 11033. (doi:10.1039/c3sm51748a)
13. Siegel GJ, Agranoff BW. 1999 Basic Neurochemistry: molecular, cellular and medical aspects. 6th edn. Philadelphia, PA: Lippincott-Raven.
14. Brochard F, Lennon JF. 1975 Frequency spectrum of the flicker phenomenon in erythrocytes. *J. De Phys*. **36**, 1035–1047. (doi:10.1051/jphys:0197500360110103500)
15. Saffman PG, Delbrück M. 1975 Brownian motion in biological membranes. *Proc. Natl Acad. Sci. USA* **72**, 3111–3113. (doi:10.1073/pnas.72.8.3111)
16. Helfrich W. 1973 Elastic properties of lipid bilayers: theory and possible experiments. *Z. Für Naturforschung C* **28**, 693–703. (doi:10.1515/znc-1973-11-1209)
17. Arroyo M, DeSimone A. 2009 Relaxation dynamics of fluid membranes. *Phys. Rev. E Stat. Nonlinear Soft Matter Phys*. **79**, 031915. (doi:10.1103/PhysRevE.79.031915)
18. den Otter WK, Shkulipa SA. 2007 Intermonolayer friction and surface shear viscosity of lipid bilayer membranes. *Biophys. J*. **93**, 423–433. (doi:10.1529/biophysj.107.105395)
19. Henle ML, Levine AJ. 2010 Hydrodynamics in curved membranes: the effect of geometry on particulate mobility. *Phys. Rev. E* **81**, 011905. (doi:10.1103/physreve.81.011905)
20. Powers TR. 2010 Dynamics of filaments and membranes in a viscous fluid. *Rev. Mod. Phys*. **82**, 1607–1631. (doi:10.1103/revmodphys.82.1607)
21. Stillwell W. 2019 Membrane transport. *PubMed Central* 423–451. (doi:10.1016/B978-0-444-63772-7.00019-1)

22. Lamparter L, Galic M. 2020 Cellular membranes, a versatile adaptive composite material. *Front. Cell Dev. Biol*. **8**. (doi:10.3389/fcell.2020.00684)
23. Al-Izzi SC, Morris RG. 2023 Morphodynamics of active nematic fluid surfaces. *J. Fluid Mech*. **957**. (doi:10.1017/jfm.2023.18)
24. Guckenberger A, Gekle S. 2017 Theory and algorithms to compute Helfrich bending forces: a review. *J. Phys.: Condens. Matter* **29**, 203001. (doi:10.1088/1361-648X/aa6313)
25. Santiago JA. 2018 Stresses in curved nematic membranes. *Phys. Rev. E* **97**, 052706. (doi:10.1103/physreve.97.052706)
26. Rangamani P, Agrawal A, Mandadapu KK, Oster G, Steigmann DJ. 2013 Interaction between surface shape and intra-surface viscous flow on lipid membranes. *BMMB* **12**, 833–845. (doi:10.1007/s10237-012-0447-y)
27. Henle ML, McGorty R, Schofield AB. 2008 The effect of curvature and topology on membrane hydrodynamics. *Europhys. Lett*. **84**, 48001. (doi:10.1209/0295-5075/84/48001)
28. Happel J, Brenner H. 1965 *Low reynolds number hydrodynamics*. Englewood Cliffs, NJ Prentice Hall.
29. Saffman PG. 1976 Brownian motion in thin sheets of viscous fluid. *J. Fluid Mech*. **73**, 593–602. (doi:10.1017/s0022112076001511)
30. Daniels DR, Turner MS. 2007 Diffusion on membrane tubes: a highly discriminatory test of the Saffman–Delbruck theory. *Langmuir* **23**, 6667–6670. (doi:10.1021/la0635000)
31. Hughes BD, Pailthorpe BA, White LR. 1981 The translational and rotational drag on a *cylinder* moving in a membrane. *J. Fluid Mech*. **110**, 349–372. (doi:10.1017/s0022112081000785)
32. Samanta R, Oppenheimer N. 2021 Vortex flows and streamline topology in curved biological membranes. *Phys. Fluids* **33**, 051906. (doi:10.1063/5.0052213)
33. Bagaria S, Samanta R. 2022 Dynamics of force dipoles in curved fluid membranes. *Phys. Rev. Fluids* **7**, 093101. (doi:10.1103/physrevfluids.7.093101)
34. Jain S, Samanta R. 2023 Force dipole interactions in tubular fluid membranes. *Phys. Fluids* **35**. (doi:10.1063/5.0151447)
35. Levine AJ, Liverpool TB, MacKintosh FC. 2004 Mobility of extended bodies in viscous films and membranes. *Phys. Rev. E* **69**, 021503. (doi:10.1103/physreve.69.021503)
36. Shi W, Moradi M, Nazockdast E. 2024 The drag of a filament moving in a supported spherical bilayer. *JFM* **979**, A6. (doi:10.1017/jfm.2023.1036)
37. Hosaka Y, Yasuda K, Okamoto R, Komura S. 2017 Lateral diffusion induced by active proteins in a biomembrane. *Phys. Rev. E* **95**, 052407. (doi:10.1103/PhysRevE.95.052407)
38. Brown FLH. 2008 Elastic modeling of biomembranes and lipid bilayers. *Annu. Rev. Phys. Chem*. **59**, 685–712. (doi:10.1146/annurev.physchem.59.032607.093550)
39. Danov KD, Dimova R, Pouligny B. 2000 Viscous drag of a solid sphere straddling a spherical or flat surface. *Phys. Fluids* **12**, 2711–2722. (doi:10.1063/1.1289692)
40. Dimova R, Danov K, Pouligny B, Ivanov IB. 2000 Drag of a solid particle trapped in a thin film or at an interface: influence of surface viscosity and elasticity. *J. Colloid Interface Sci*. **226**, 35–43. (doi:10.1006/jcis.2000.6710)
41. Dimova R, Dietrich C, Hadjiisky A, Danov K, Pouligny B. 1999 Falling ball viscosimetry of giant vesicle membranes: finite-size effects. *EPJ B* **12**, 589–598. (doi:10.1007/s100510051042)
42. Shi W, Moradi M, Nazockdast E. 2022 Hydrodynamics of a single filament moving in a spherical membrane. *Phys. Rev. Fluids* **7**, 084004. (doi:10.1103/PhysRevFluids.7.084004)
43. Komura S, Andelman D. 2014 Physical aspects of heterogeneities in multi-component lipid membranes. *Adv. Colloid Interface Sci*. **208**, 34–46. (doi:10.1016/j.cis.2013.12.003)
44. Naji A, Brown FLH. 2007 Diffusion on ruffled membrane surfaces. *J. Chem. Phys*. **126**, 235103. (doi:10.1063/1.2739526)
45. Almendro-Vedia V, Natale P, Valdivieso González D, Lillo MP, Aragones JL, López-Montero I. 2021 How rotating ATP synthases can modulate membrane structure. *Arch. Biochem. Biophys*. **708**, 108939. (doi:10.1016/j.abb.2021.108939)
46. Oppenheimer N, Diamant H. 2009 Correlated diffusion of membrane proteins and their effect on membrane viscosity. *Biophys. J*. **96**, 3041–3049. (doi:10.1016/j.bpj.2009.01.020)
47. Morris RG, Turner MS. 2015 Mobility measurements probe conformational changes in membrane proteins due to tension. *Phys. Rev. Lett.* **115**, 198101. (doi:10.1103/PhysRevLett.115.198101)

48. Baranova N, Radler P, Hernández-Rocamora VM, Alfonso C, López-Pelegrín M, Rivas G, Vollmer W, Loose M. 2020 Diffusion and capture permits dynamic coupling between treadmilling FtsZ filaments and cell division proteins. *Nat. Microbiol*. **5**, 407–417. (doi:10.1038/s41564-019-0657-5)
49. Nguyen ZH, Atkinson M, Park CS, Maclennan J, Glaser M, Clark N. 2010 Crossover between 2D and 3D fluid dynamics in the diffusion of islands in Ultrathin freely suspended smectic films. *Phys. Rev. Lett*. **105**, 268304. (doi:10.1103/physrevlett.105.268304)
50. Pak OS, Lauga E. 2014 Generalized squirming motion of a sphere. *J. Eng. Math*. **88**, 1–28. (doi:10.1007/s10665-014-9690-9)
51. Dorrepaal JM. 1978 The Stokes resistance of a spherical cap to translational and rotational motions in a linear shear flow. *J. Fluid Mech*. **84**, 265. (doi:10.1017/s0022112078000154)
52. Kim S, Karrila SJ. 2013 *Microhydrodynamics: principles and selected applications*. Oxford, UK: Butterworth-Heinemann.
53. Happel J, Brenner H. 2012 *Low Reynolds number hydrodynamics: with special applications to particulate media*. Berlin, Germany: Springer Science & Business Media.
54. Rey AD. 2006 Polar fluid model of viscoelastic membranes and interfaces. *J. Colloid Interface Sci*. **304**, 226–238. (doi:10.1016/j.jcis.2006.08.027)
55. Riley KF, Hobson MP, Bence SJ. 2006 *Mathematical methods for Physics and Engineering: a comprehensive guide*. Cambridge, UK: Cambridge University Press.
56. Arfken G. 1985 *Mathematical methods for Physicists*. 3rd edn. San Diego, CA: Academic Press.